Stress Field Simulation and Its Experimental Verification of Carburizing-Quenching Process Performed on 18CrNiMo7-6 Steel

Shengwei QIN *, Haiyang MA, Lianxiang WANG

School of Mechanical and Power Engineering, Zhengzhou University, Henan Province 450001, P.R. China

https://doi.org/10.5755/j02.ms.30932

Received 29 March 2022; accepted 01 June 2022

The carburizing and quenching process of 18CrNiMo7-6 steel was performed through simulation methods and experiments. The study was carried out to accurately predict the residual stress distribution of carburized samples after the quenching process. The stress and retained-austenite amount were measured via X-ray diffraction. Similarly, the carbon content was determined using a carbon sulfur analyzer, respectively. A detailed model with the coupling of thermal, metallic, and mechanical fields was built to predict the evolution of the stress field during the quenching process. The carburized "thoroughly" specimens at different carbon potentials were used to obtain the required mechanical property parameters and dilatometric parameters for FEM simulation. According to the results, the martensite transformation kinetic parameters α value of 18CrNiMo7-6 alloy steel should be 0.0202. With the increase of carbon content, the changing trend of the transformation plasticity coefficient K appeared as a 'tick' shape. A compressive residual stress field was generated at the carburized layer surface after the quenching process, and the maximum value of 340 MPa occurred at ~ 0.9 mm below the surface. The carbon profile and residual stress fields predicted from the FEM simulation corresponded closely to the experimentally determined results.

Keywords: carburizing and quenching process, residual stress, finite simulation method, martensitic transformation.

1. INTRODUCTION

Carburizing and quenching are widely used for improving the mechanical properties of mechanical components, such as the gear ring or shaft. When machine parts are carburized and quenched, a typical carburized layer, with a small amount of retained austenite, a large amount of martensite, and carbon-content gradient along the layer depth, is formed at the surface. The diffusionless martensite transformation with volume expansion occurs in the carburized layer during the quenching process, and exerts a significant effect on the performance of machine parts. Furthermore, the order of the martensite transformation varies with position in the carburized layer, owing to the gradient carbon content, which yields a hardness and stress field distribution that varies with the depth in the layer. The fatigue resistance and wear property of this part can be significantly increased, owing to the residual compressive stress induced by heat treatment on the part surface [1]. Studies on the stress distribution after the carburizing and quenching process are therefore warranted.

Many models of the residual stress field associated with the carburizing and quenching process have been established by means of the finite element method. S. Denis et al. developed a phase transformation model which coupled to the calculation of temperature, stress and strain evolutions in a massive specimen submitted to carbon gradients [2]. Ferro et al. [3] and Song et al. [4] found that compressive residual stress at the surface of a part was generated after the martensitic transformation at the core of the part. This was attributed to the combination of a temperature gradient and the mismatch in Ms between the outer and the interior of the part. The simulation accuracy of the residual stress after carburizing and quenching process is closely related to the transformation of austenite during the quenching process, which is affected by the accuracy of the kinetic parameters of martensite transformation in the K-M formula [5]. Another parameter that affects the accuracy of residual stress is transformation plasticity. Rangaswamy et al. simulated the residual stress distribution of a 5120 steel carburized disc [6]. However, the transformation plasticity was neglected, resulting in significant discrepancies between the experimental value and the simulated value. Greenwood and Johnson [7], Abrasart, Leblond [8-9], Desalos and others have proposed different calculation models for transformation plasticity. The Desalos model is widely used in finite element software, and is also the model used in this research. In the Desalos model, the transformation plasticity coefficient K is of great importance [10, 11]. Much of the previous work was devoted to determining the K value of an alloy with a fixed composition [12], besides the K value was considered to be slightly affected by chemical composition [2]. The effect of carbon content on the phase change plasticity coefficient K in carburized steel is rarely studied. Moreover, the simulation results in some studies have not been verified by corresponding experiments. Lingamanaik et al. developed a thermo-mechanical finite element model to predict the inhomogeneous martensitic transformation [13]. The results showed that the surface carbon content, depth of the case-hardened layer, and compressive stresses at the fillet of the gear tooth can be increased by increasing the carburization time. However, the numerical simulation results were discussed without experimental verification via (for

* Corresponding author. Tel.: +86-18137129321.
Email: *qinsw@zzu.edu.cn* (S. Qin)

example) carbon profiles and the residual stress distribution. In addition, in many studies, the mechanical property parameters used for calculating the residual stress were obtained using empirical or semi-empirical formulas rather than experimental measurements [14].

In order to accurately simulate the distribution of residual stress employing the finite element method, the martensite transformation kinetic parameters α value and the transformation plasticity coefficient K were measured by using the 'thoroughly' carburized samples with different carbon contents. Moreover, 18CrNiMo7-6 steel was subjected to a typical carburizing and quenching process, and the above issue was investigated by comparing the experimental results with simulated values.

2. EXPERIMENTAL PROCEDURES

2.1. Experimental materials and methods

The chemical compositions of the studied steel are listed in Table 1. The hot-rolled plate (thickness: 200 mm) of 18CrNiMo7-6 steel was prepared by Shaoguan Zhongji Heavy Industry Co. Ltd., Guangdong, China. Moreover, the cylindrical specimens with a diameter of 16.72 mm and a length of 130 mm were prepared for verification of the carbon content, microstructure, and residual stress distribution after the carburizing and oil-quenching process.

Table 1. Chemical composition of the 18CrNiMo7-6 steel, wt.%

C	Si	Mn	Cr	Ni	Mo	Fe
0.21	0.34	0.72	1.58	1.4	0.26	Bal.

The carbon content was determined by using a NJFY-CS100A carbon sulfur analyzer. The material that needed to be burned at different depths was prepared by the mechanical stripping method with a feed of 0.1 mm. The X-ray diffraction (XRD), with CuKα radiation using a D/max-2550 X-ray diffractometer, was used to detect the volume fraction of retained austenite. The fractions were obtained through a direct comparison of the integrated intensity measured for the martensite (200)α and (211)α peaks and the austenite (200)γ, (220)γ, and (311)γ peaks. The same carburizing process was performed on the cylindrical sample and the plate sample. Taking the carbon content as the contact point, the two types of samples have the same austenite content at depths with the same carbon content. In addition, the residual stress was measured by means of XRD (iXRD combo, Proto Company, Ontario, Canada) with Cr radiation (λ = 0.2291 nm). The principle of the X-ray residual stress tester is that microscopic strain will occur in the material lattice under the action of macroscopic stress, and the diffraction Angle of the lattice will change. According to the microscopic strain, the value of macroscopic residual stress can be inversely derived. In the two-dimensional plane stress state, σ_ϕ is expressed as:

$$\sigma_\phi = K \frac{\partial 2\theta_{\phi\Psi}}{\partial \sin^2 \Psi}, \quad (1)$$

where K is the stress constant, which can be expressed by Eq. 2. $2\theta_{\phi\Psi}$ is the diffraction angle, measured by the diffraction device; Ψ is the azimuth of the diffraction crystal plane.

$$K = -\frac{E}{2(1+\nu)} \cdot \frac{\pi}{180} \cdot \cot\theta_0, \quad (2)$$

where E is Young's modulus; ν is Poisson's ratio; θ_0 is Bragg angle under no stress state.

Cr target was selected for measurement, and the diffraction plane was (211). X-ray penetration is low (usually several microns to tens of microns), so only the surface residual stress can be measured. To test the residual stress distribution with the direction of depth, the sample was stripped by electrochemical corrosion method with saturated salt water as the corrosion solution, the stripping voltage and stripping time were 60 V/10 s, and the stripping depth was 100 um. The residual stress values at three positions are measured in each layer and the average value was taken as the final result.

The mechanical property parameters of the materials at different positions of the carburized layer were determined via axial tensile testing on DIL 805A/D/T Quenching & Deformation Dilatometers. The samples to be tested (with a carbon content of 0.21 %, 0.49 %, 0.65 %, and 0.85 %) were obtained by means of a solid carburizing and diffusion process. The samples were placed in a ceramic crucible containing 100 g of pure charcoal powder, and kept at 925 °C for 0 h, 0.5 h, 3 h, and 6 h. The samples were taken out and kept in a vacuum furnace at 950 °C for 6 hours. The carbon content on the surface of the sample and the core of the sample were the same as measured by NJFY-CS100A carbon sulfur analyzer. The hardness and XRD results showed that the carbon content of the surface was also consistent with that of the core. In other words, the samples were carburized "thoroughly". Finally, the martensite specimens with different carbon content were subjected to full quenching to -100 °C.

As an example, the stress-strain curves of martensite specimen with a carbon content of 0.2 % were measured as follows: The martensite specimens were tested at 25 °C, 100 °C, 200 °C, 300 °C, and 400 °C at a heating rate of 20 °C/s. For the stress-strain test (deformation rate: 0.001/s) of austenite, the specimen was heated to 1000 °C for 30 s, then cooled to 900 °C, 800 °C, 700 °C, 600 °C, and 500 °C at a cooling rate of 50 °C/s. A short isothermal time (5 s) was set during the tensile test before deformation, to prevent the formation of tempered martensite and the decomposition of supercooled austenite. The same test method was used for other samples with different carbon contents, except that the deformation temperatures were different.

2.2. Conditions of experiment and simulation

The heat treatment (HT) process is shown in Table 2. The carburizing and quenching process was performed in continuous furnaces. The carburizing and diffusing time as well as temperature, were 350 min and 180 min, 920 °C and 900 °C, respectively. The carbon concentration of the furnace atmosphere was 1.15 wt.% during carburization and 0.95 wt.% during the subsequent diffusion process. Afterward, the temperature and carbon concentration decreased to 840 °C and 0.80 wt.%, respectively. In the final step of the process, the specimens were immersed in oil quenchant at 80 °C. The carburizing and quenching simulation of the specimen, including the temperature,

microstructure and stress fields, is performed on the Deform-HT software.

Table 2. Schematic of the carburizing process

Stage	Time, h	Temperature, ℃	Carbon atmosphere, %C
1	01:00	850	0.6
2	00:05	920	1.15
3	05:50	920	1.15
4	00:05	900	0.95
5	03:00	900	0.95
6	00:05	840	0.8

A two-dimensional (2-D) axisymmetric finite element model of the carburized sample was used for simulation. This model corresponded to the center of the cylindrical specimens. The length-to-diameter ratio was > 6 and, hence, the cylindrical specimens can be considered infinitely long. The model was meshed by quadrilateral elements with four nodes. Thus, a model with 7224 nodes and 7110 elements was established.

3. MODELS FOR CARBURIZING AND QUENCHING PROCESS

3.1. Carburizing process

The carburizing process is a non-steady-state diffusion process. The carburizing process can be described by Fick's second law, which is given as [16]:

$$\frac{\partial C}{\partial t}=\frac{\partial}{\partial x}(D\frac{\partial C}{\partial x}) \quad , \tag{3}$$

where C is the carbon content of the carburized layer in %, t is the carburizing time, and x is the Cartesian coordinate. The diffusion coefficient D is related to the temperature T, carbon content, and alloying elements M in the diffusion process of multi-component alloy steel [17].

$$D(T,M,C)=(0.146-0.036C(1-1.075Cr)+\sum k_1M) \cdot\exp(-\frac{144.3-15.0C+0.37C^2+\sum k_2M}{RT}) \quad , \tag{4}$$

where Cr is the mass fraction of chromium; M is the mass fraction of alloying element in %; R is the molar gas constant; k_1 and k_2 are constants of alloy elements, and their values are shown in Table 3.

Table 3. Alloying elements and alloying parameters of diffusion coefficient model

M	Mn	Si	Ni	Cr	Mo	Al
k_1	-0.0315	0.0509	-0.0085	0.0*	0.3031	-0.0520
k_2	-4.3663	4.0507	-1.2407	7.7260	12.1266	-6.7886
* is considered in the previous exponential section						

The external boundary condition is expressed as:

$$-D\left(\frac{\partial C}{\partial x}\right)_{x=0}=\beta(\mathrm{C}_\infty-\mathrm{C}_s) \quad , \tag{5}$$

where C_∞ stands for the environmental carbon potential, and C_s denotes the carbon content of the steel. Both units of C_∞ and C_s are %.

The temperature-dependent transfer coefficient of the steel, β, can be expressed as:

$$\beta=\beta_0\exp(-\frac{E}{RT}) \quad , \tag{6}$$

where E is the activation energy of the reaction.

3.2. Quenching process

3.2.1. Temperature field

During the carburizing quenching process, the temperature field was controlled by the Fourier heat equation coupled with latent heat due to martensitic transformation.

$$\lambda\left(\frac{\partial^2T}{\partial r^2}+\frac{1}{r}\frac{\partial T}{\partial r}+\frac{1}{r^2}\frac{\partial^2T}{\partial\varphi^2}+\frac{\partial^2T}{\partial z^2}\right)+q=\rho\cdot C_p\frac{\partial T}{\partial t} \quad , \tag{7}$$

where ρ is the density (taken as 7850 kg/m3); c is the specific heat and k is the thermal conductivity, respectively, which are calculated by the Jmatpro software [18]; q is the internal heat source.

The initial temperature was set as 840 °C and the quenching oil temperature was 100 °C. The boundary condition of heat transfer was given as follows:

$$-\lambda\frac{\partial T}{\partial n}\Big|_s=h\left(T_w-T_f\right) \quad , \tag{8}$$

where T_w and T_f are the temperature of the cylinder surface and the quenching oil, respectively; n is the normal direction of the outer boundary. The heat transfer coefficient h between 18CrNiMo7-6 and KR128 is adopted from data reported in the literature1 [1].

3.2.2. Microstructure field

The martensite transformation is a diffusionless phase transformation, which depends only on the temperature. The K-M equation is used to describe this transformation and is given as follows [5]:

$$\xi_M=1-\exp[-\alpha(M_s-T)] \quad , \tag{9}$$

where ξ_M is the volume fraction of martensite; M_s is the starting temperature of martensitic transformation; α is a proportionality coefficient, reflecting the speed of martensite transformation, which varies with the type of steel, respectively. The M_s and α values of the materials in different depths of the carburized layer were obtained from our measurement.

3.2.3. Stress field

Quenching is a non-linear thermoplastic process, which can be described by the incremental theory. The total strain rate $\{\dot{\varepsilon}_{ij}\}$ includes the rate of elastic strain $\{\dot{\varepsilon}^e_{ij}\}$, plastic strain $\{\dot{\varepsilon}^p_{ij}\}$, thermal strain $\{\dot{\varepsilon}^{th}_{ij}\}$, phase transformation strain $\{\dot{\varepsilon}^{tr}_{ij}\}$, and transformation plasticity strain $\{\dot{\varepsilon}^{tp}_{ij}\}$. The total strain rate $\{\dot{\varepsilon}_{ij}\}$ is then given as [19, 20]:

$$\dot{\varepsilon}_{ij} = \dot{\varepsilon}_{ij}^{e} + \dot{\varepsilon}_{ij}^{p} + \dot{\varepsilon}_{ij}^{th} + \dot{\varepsilon}_{ij}^{tr} + \dot{\varepsilon}_{ij}^{tp}, \quad (10)$$

Assuming that the hardening rule is isotropic, the Von Mises yield criterion was adopted as the yield function type. The model of plastic flow stress σ_p, which considers the effect of strain ε, carbon content, and temperature, is described by [20]:

$$\dot{\varepsilon}_{ij}^{p} = \dot{G}\left(\frac{\partial F}{\partial \sigma_{kl}}\dot{\sigma}_{kl} + \frac{\partial F}{\partial T}\dot{T} + \sum \frac{\partial F}{\partial \xi_{IJ}}\dot{\xi}_{IJ} + \frac{\partial F}{\partial C}\dot{C}\right)\frac{\partial F}{\partial \sigma_{ij}}$$

$$\frac{1}{\hat{G}} = -\left[\frac{\partial F}{\partial \varepsilon_{mn}^{p}} + \frac{\partial F}{\partial k}\sigma_{mn}\right]\frac{\partial F}{\partial \sigma_{mn}}$$

$$F \equiv \mathrm{f}\left(T, C, \sigma_{ij}, \varepsilon_{ij}^{p}, \xi_{I}, k\right), \quad (11)$$

where F is the yield equation based on the mixed phase; T is the temperature; C is the carbon content; σ_{ij} is the flow stress; ε_{ij}^{p} is plastic strain; ξ_I is phase microstructure; K is the hardening parameter.

The elastic strain rate $\dot{\varepsilon}_{ij}^{e}$ can be expressed as:

$$\dot{\varepsilon}_{ij}^{e} = \frac{1+\nu}{E}\dot{\sigma}_{ij} - \frac{\nu}{E}\dot{\sigma}_{kk}\delta_{ij}, \quad (12)$$

where E and ν are elasticity modulus and Poisson's ratio, respectively, depending on both the temperature and carbon content, were obtained from the stress-strain curves of martensite and austenite. σ_{ij} is the flow stress and δ_{ij} is the Kronecker delta.

The strain rate tensor components can be written as [20, 21]:

$$\dot{\varepsilon}_{ij}^{th} = \alpha(C)\Delta\dot{T}\delta_{ij}; \quad (13)$$

$$\dot{\varepsilon}_{ij}^{tr} = \sum \beta_{IJ}(C,T)\dot{\xi}_{IJ}\delta_{ij}; \quad (14)$$

$$\dot{\varepsilon}_{ij}^{tp} = \frac{3}{2}K_{IJ}h(\xi_{IJ})\dot{\xi}_{IJ}S_{ij}, \quad (15)$$

where α is the thermal expansion coefficient. β_{IJ} is the coefficient of phase transformation in fraction length change due to the phase change from phase I to phase J, $\dot{\xi}_I$ is the volume fraction rate of the phase transformation, where the transformation volume fraction from phase I to phase J is differentiated with respect to time. K_{IJ} denotes the transformation plasticity coefficient, and normalized function $h(\xi_{IJ}) = 2(1-\xi_{IJ})$ represents the contribution from transformation progress to the transformation plasticity strain [20, 21]. The mechanical property parameters of the materials at different positions of the carburized layer were obtained from our measurement.

4. RESULTS

4.1. Martensite transformation kinetic parameter

M_s, and α (see Table 4) were determined using dilatometry. From Table 4, we find that the M_s is related to the carbon content (mass content), and as the carbon content increases, the temperatures decrease. When the carbon content in the sample is 0.21 %, M_s is 387 ℃, and when the carbon content increases to 0.82 %, M_s reduces to 113 ℃. Therefore, the higher the carbon content is, the more the austenite is retained after quenching. As for the α value in the K-M formula, it can be obtained by fitting the expansion curve. The α values of the C 0.21 %, C 0.34 %, C 0.56 %, and C 0.66 % samples are 0.0195, 0.0207, 0.0201, and 0.0205, as shown in Table 4. The values are significantly higher than other scholars' recommended values [10]. The M_f temperatures of the C 0.73 %, C 0.82 % samples are lower than the cooling temperature limit of the dilatometer (50 °C), as a result, the martensite transformation is incomplete, and the α value cannot be directly obtained. Besides, it changes slightly with the carbon content. The α values of the C 0.73 %, C 0.82 % samples can be taken as the average of the previous four samples.

Table 4. Values of M_s and α

Carbon content, %	M_s, ℃	α
0.21	387	0.0195
0.34	292	0.0207
0.56	212	0.0201
0.66	182	0.0205
0.73	148	0.0202
0.82	133	0.0202

4.2. Transformation plasticity coefficients

The mechanical property parameters used in the simulation can be obtained from the stress-strain curves of martensite and austenite. As for samples with carbon content of 0.21 %, 0.34 %, 0.56 %, 0.66 %, 0.73 % and 0.82 %, transformation plasticity coefficients K_{IJ} of 7.16, 6.65, 5.43, 5.54, 5.82 and 6.01e^{-5} MPa^{-1} are obtained respectively. As the carbon content increases, the changing trend of K_{IJ} appears as a 'tick' shape, as shown in Fig. 1.

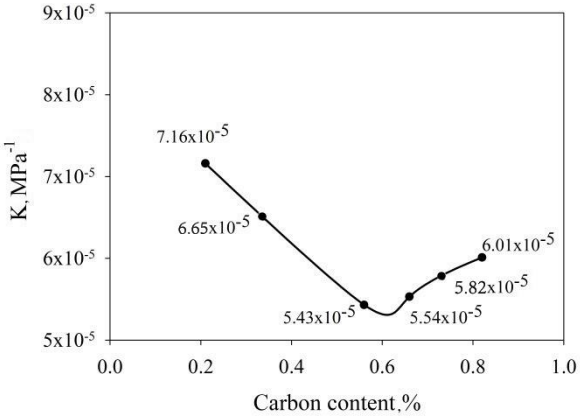

Fig. 1. Transformation plasticity coefficient K of different carbon content samples

In different carbon content ranges, the dominant mechanism of transformation plasticity is different. When the carbon content is below 0.5 %, the Greenwood and Johnson mechanism dominates. Due to the different densities of the mother phase austenite and the child phase martensite, the volume change caused by the martensite transformation process leads to the plastic deformation of

the weak phase austenite in the vicinity of the phase transition zone, and the austenite's yield strength will increase with the increase of carbon content. When the yield strength increases faster than the volume change, the *K* value will decrease with the increase of carbon content. However, when the carbon content is higher than 0.5 %, the Magee mechanism dominates. At high carbon content, lamellar martensite is mainly generated, and the lamellar martensite under no stress is randomly distributed in different directions, and the shear stresses generated also cancel out each other; under the situation with stress, the lamellar martensite will be preferentially oriented, and the microscopic plastic deformation changes into the macroscopic plastic deformation, thereby forming transformation plasticity. As the carbon content rises, the amount of lamellar martensite increases, resulting in the growth of the *K* value [22].

4.3. Carbon diffusion

Fig. 2 shows the carbon profiles determined via combustion burnout techniques performed on the carburized layer (thickness: ~ 2.0 mm) of the samples. The carbon content at the surface increases from 0.21 wt.% to 0.8 wt.%, and decreases with decreasing depth of the layer. In addition, carburizing simulation was performed in Deformed-HT [23, 24]. A two-dimensional axisymmetric finite element model was used to simulate carburizing samples. The model corresponds to the center of a cylindrical specimen. The aspect ratio was greater than 6, so the cylindrical specimen can be regarded as infinitely long. The model was meshed by the quadrilateral element with four nodes. The corresponding mechanical properties and expansion coefficient parameters were input, and carburizing temperature and carbon potential were also set. The result has been shown in Fig. 2.

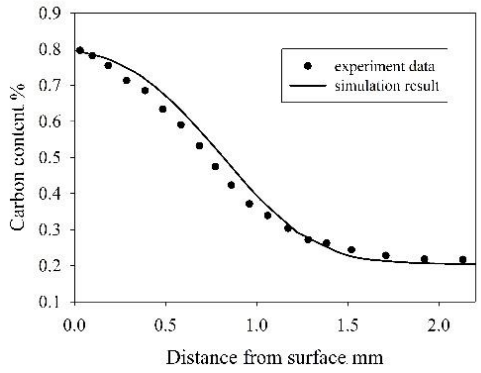

Fig. 2. Carbon content distribution of the carburized specimen

As desired, the predicted carbon content profiles decrease monotonically from 0.81 wt.% to 0.21 wt.%. As the figure shows, the simulated carbon content distribution of the carburized layer corresponds closely to the experimentally determined distribution. This correspondence indicates that the model used in the present work is quite suitable for simulating the carburizing process of 18CrNiMo7-6 steel.

Fig. 3 and Fig. 4 show the microstructure of carburized and uncarburized samples. For the carburizing sample, it can be seen that the carburizing surface contains a large number of retained austenite and lath martensite (Fig. 3 a), while the core was basically composed of martensite (Fig. 3 b). For the uncarburized sample, the microstructure of the surface (Fig. 4 a) and core (Fig. 4 b) were martensite.

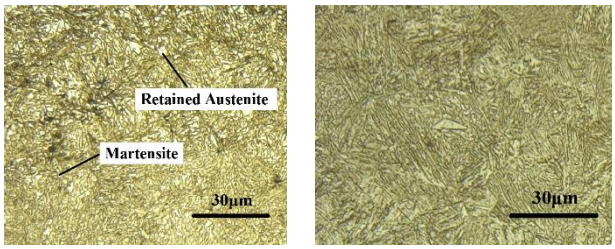

a b

Fig. 3. Microstructure of carburized sample

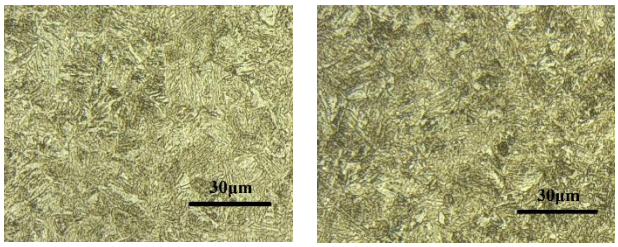

a b

Fig. 4. Microstructure of uncarburized sample

4.4. Retained austenite

The volume fraction distribution of retained austenite along the depth was detected via XRD, as shown in Fig. 5.

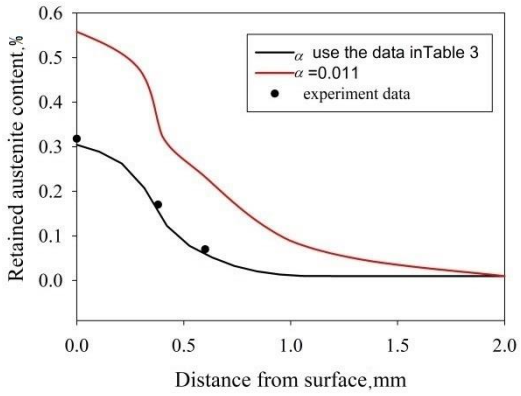

Fig. 5. Distribution of retained austenite in the carburized specimen

In general, the volume fraction decreases with decreasing depth of the carburized layer, with the maximum content (33 vol.%) occurring on the layer surface. A limited amount (2 – 4 vol.%) of retained austenite is present at a depth of 1.0 mm. The remaining carburized-layer microstructure is composed of martensite. The K-M equation 4 [16] indicates that the volume fraction of austenite decreases monotonically with decreasing carbon content. Consider the surface layer of the sample with a carbon content of 0.8 wt.%. Even if the temperature is cooled to room temperature, which is still higher than the M_f, a considerable amount of retained austenite can exist stably.

4.5. Residual stress

The residual stress fields of the carburized specimens after the quenching process are determined, as shown in Fig. 6. The residual stress is determined from the surface to a depth of 2.5 mm. The residual compressive stress is generated in the carburized layer, with stresses of ~ 100 MPa occurring on the carburized surface. The maximum stress of 340 MPa is produced at ~ 0.9 mm below the surface. Moreover, the crossover from compressive stress to a tensile stress of the specimen occurs at ~ 2.0 mm. The residual compressive stress generated on the workpiece surface can yield a significant improvement in the fatigue strength and service life of the workpiece [25, 26].

The simulated residual stress fields of the carburized specimens are shown in Fig. 6. The simulated residual stress fields in the carburized layers of the specimen concur with the experimental data. This indicates that the model and mechanics property parameters used in this work are quite suitable for simulating the quenching process of the carburized 18CrNiMo7-6 steel.

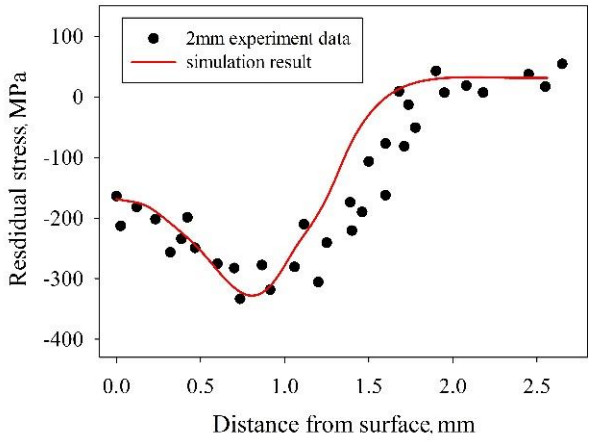

Fig. 6. Comparison of the measured and calculated residual stress values

5. DISCUSSION

5.1. Determinants of retained austenite content

The value of α in Eq. 7 has a great influence on the simulation accuracy of the retained austenite content after the quenching process. The α values of the samples are significantly higher than other scholars' recommended value of 0.011 [10], as shown in Table 4. Fig. 5 shows the retained austenite content after the quenching process when α is taken as 0.011 and 0.0202 respectively. It is found from Fig. 4 that when α takes 0.0202, the simulated value of retained austenite is close to the actual measured value; when α takes 0.011, the retained austenite content is significantly higher than the actual measured value. The less the amount of austenite transformation is, the smaller the stress caused by the phase transition will be, which results in a reduction of the residual compressive stress. The difference in α value is caused by the difference in the chemical composition of different materials. Therefore, for 18CrNiMo7-6 alloy steel, the α value should be taken as 0.0202.

5.2. Determination of transformation plasticity coefficient

To study the influence of the transformation plasticity coefficient on the residual stress, two K values were used in the simulation, namely $K = 0$ (without considering the transformation plasticity coefficient) and the K value of samples with different carbon content measured by the experiment. The simulation results are shown in Fig. 7 in black and the red curve. It can be seen that the red curve is more consistent with the experimentally measured values; and the difference between the simulated results at $K = 0$ and the actual measured value is larger, besides the residual compressive stress increases significantly; This is due to the relaxation effect of transformation plasticity [27]. For a carburized sample, as martensitic transformation develops last in the surface area, the associated stress relaxation effect occurs until the end of the cooling. Ignoring the transformation plasticity ($K = 0$, that is, the black line) will cause the residual compressive stress to increase significantly. The transformation plasticity coefficient K of the samples varies with different carbon content, and the relaxation effect on the residual stress is also different. In a word, the phase change transformation plasticity coefficient K varied with carbon content, and it has a great influence on the residual stress distribution.

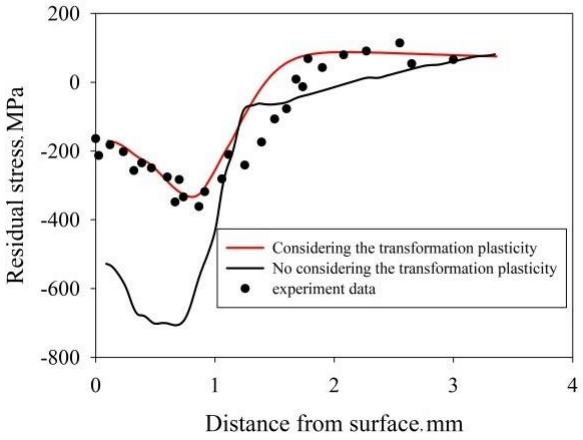

Fig. 7. Comparison of the residual stress values with a different K value

5.3. The evolution of stress

The complexity of the residual stress distribution depends on not only the thermal stress caused by the temperature difference between the outer and the interior of the specimen but also the structural stress caused by the large volume expansion associated with martensite transformation. Moreover, the carbon content of the surface comprising the carburized layer is higher than that of the core and, hence, the martensite transformation temperatures of the surface is lower than that of the core. This leads to a different order of martensite transformation in the carburized layer. Therefore, for the carburized specimen, the transformation may occur first in the interior rather than in the carburized surface. The evolution of stress is elucidated by using the FEM to predict the variation in the temperature field (Fig. 8) and transient stress (Fig. 9) of the specimen.

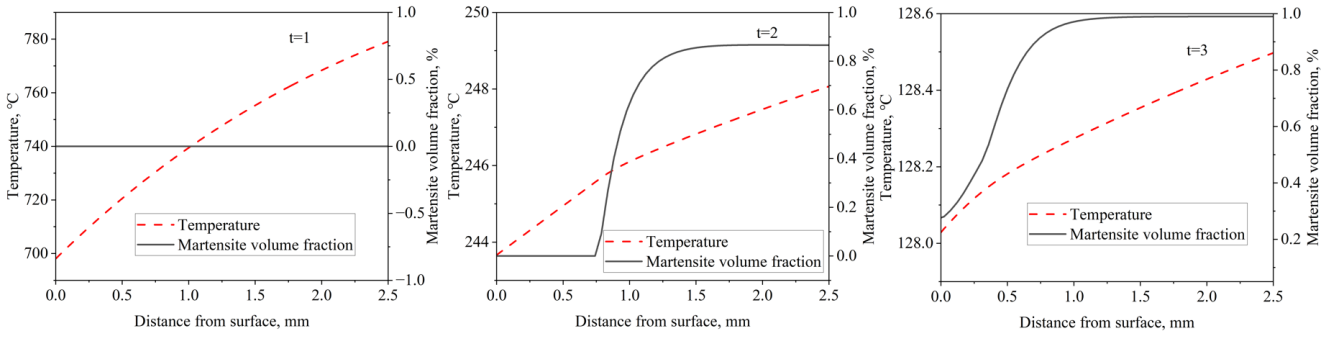

Fig. 8. Temperature distribution of carburized specimen at different cooling stages

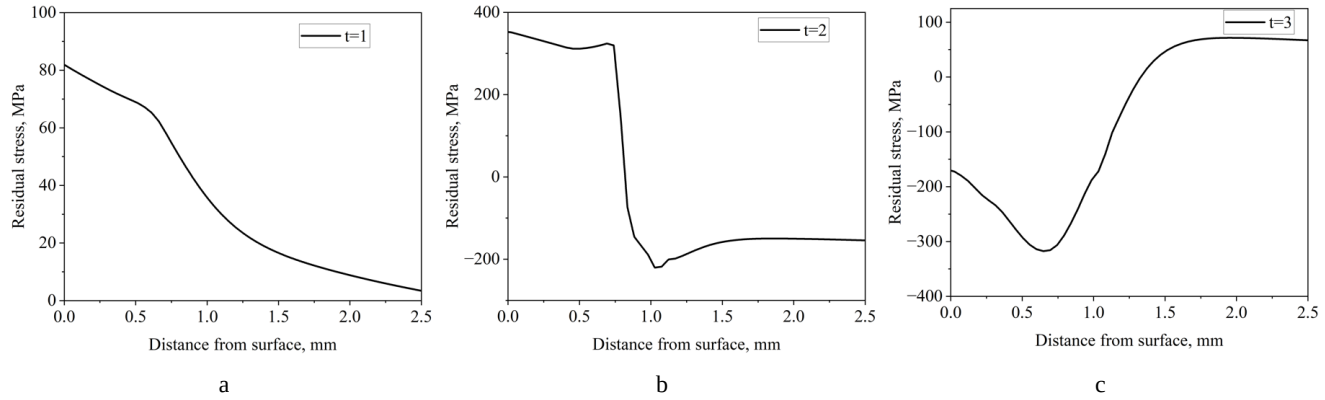

Fig. 9. Simulated stress distribution of carburized specimen at different quenching stages

The order of the different quenching stages is denoted as $t = 1, 2, 3$. At the beginning of the quenching process ($t = 1$), a tensile stress is generated in the carburized surface, the temperature of the whole specimen is above the martensite transformation temperature. The stress shown in Fig. 9 a is the thermal stress, i.e., the tensile stress generated on the surface of the sample due to the large degree of shrinkage. Furthermore, the temperature reduction of the surface is higher than that of the core, thereby leading to an increase in the tensile stress. With progression of quenching ($t = 2$), see Fig. 9 b, the austenite in the core transforms to martensite with high volume expansion, but the austenite in the surface remains unchanged. This difference in microstructure results from the difference between the Ms values of the surface and the core. Hence, the compressive stress generated in the core of the specimen (see Fig. 9 b). When the temperature decreases ($t = 3$), the martensite transformation occurs near the surface layer, and a compressive stress is generated. Furthermore, the zone in the interior, which has transformed to martensite, hinders the volume expansion from the surface, and the compressive stress in the core is thereby reduced (see Fig. 9 c). The corresponding stress field in the specimen cooled to room temperature can be considered the residual stress field, where the maximum compressive stress occurs at ~ 0.9 mm below the surface of the specimen. Yang et al. [28] explained that the carbon content of the surface area varies only slightly and, hence, the martensite transformation temperatures of this area are quite similar. Moreover, the temperature of the outer layer decreases more rapidly than the temperature of the interior, leading to martensite transformation from the outermost surface. The maximum compressive stress is therefore generated in the sub-surface region (rather than at the surface). In addition, based on the distribution of the retained-austenite content, the trends are further interpreted as follows: Generally, Ms decreases with increasing carbon content, which is highest at the specimen surface, where martensite transformation occurs last. The maximum residual compressive stress should occur at the surface. However, compared with the core of the carburized specimen, the outer surface contained a larger amount of austenite retained after quenching (see Fig. 5), thereby reducing the amount of residual compressive stress generated. The maximum compressive stress is therefore produced in the inner surface, i.e., below the surface, as shown in Fig. 9 c.

6. CONCLUSIONS

In this work, the residual stress of a 18CrNiMo7-6 steel after a carburizing and quenching process was investigated by means of experimental and finite element methods. A detailed model coupling the thermal, metallic, and mechanical fields was built to predict the internal stress and residual stress field. The main conclusions of this study are summarized as follows:

1. The corresponding mechanical property parameters and dilatometric parameters for FEM simulation are determined via accurate measurements. The martensite transformation kinetic parameters α value should be 0.0202 instead of 0.011 for 18CrNiMo7-6 alloy steel.

The difference in α value is caused by different chemical composition. As carbon content growths, the changing trend of the transformation plasticity coefficient K appears as 'tick' shape. The dominant mechanism of K in different ranges of carbon content is different. The predicted residual stress fields correspond closely to the experimentally determined data for the carburized and quenched specimen.

2. After the carburizing and quenching process, a compressive residual stress field is obtained in the 18CrNiMo7-6 specimen, and the stress is distributed in the carburized layer in the form of a tick. The maximum compressive residual stress value of 340 MPa occurs at ~ 0.9 mm below the surface of the specimen. The crossover from compressive stress to tensile stress of the specimen occurs at ~ 2.0 mm.
3. Analysis of the stress evolution during the quenching process revealed that the stress distribution of the carburized layer is subjected to the combined action of a thermal stress and a structural stress. Furthermore, the formation of the final residual compressive stress is related to the order of the martensite transformation in different carburized-specimen layers. In addition, the difference in the amount of transformed austenite results in the transfer of the maximum residual compressive stress from the surface to the interior.

Acknowledgments

This work was financially supported by the National Natural Science Foundation of China (No. 52001281, No. U1804254) and Key Scientific and Technological Research Projects in Henan Province (No. 192102210012).

REFERENCES

1. **Liu, L., Li, Q., Liu, X., Gao, Y., Ren, X., Liao, B., Yang, Q.** Stress Field Simulation of Carburized Specimens with Different Carbon Content during Quenching Process *Materials Letters* 61 2007: pp. 1251 – 1255. https://doi.org/10.1016/j.matlet.2006.07.024
2. **Denis, S., Archambault, P., Aubry, C., Mey, A., Louin, J., Simon, A.** Modelling of Phase Transformation Kinetics in Steels and Coupling with Heat Treatment Residual Stress Predictions *Journal de Physique IV* 9(PR9) 1999: pp. 323 – 332. https://doi.org/10.1051/jp4:1999933
3. **Ferro, P., Porzner, H., Tiziani, A., Bonollo, F.** The Influence of Phase Transformations on Residual Stresses Induced by the Welding Process – 3D and 2D Numerical Models *Modelling and Simulation in Materials Science and Engineering* 14 2006: pp. 117. https://doi.org/10.1088/0965-0393/14/2/001
4. **Song, G., Liu, X., Wang, G., Xu, X.** Numerical Simulation on Carburizing and Quenching of Gear Ring *Journal of Iron and Steel Research International* 14 2007: pp. 47 – 52. https://doi.org/10.1016/S1006-706X(07)60089-2
5. **Koistinen, D.P., Marburger, R.E.** A General Equation Prescribing the Extent of the Austenite-martensite Transformation in Pure Iron-carbon Alloys and Plain Carbon Steels *Acta Metallurgica* 7 1959: pp. 59 – 60. https://doi.org/10.1016/0001-6160(59)90170-1
6. **Rangaswamy, P., Scherer, C.P., Bourke, M.** Experimental Measurements and Numerical Simulation of Stress and Microstructure in Carburized 5120 Steel Disks *Materials Science and Engineering: A* 298 2001: pp. 158 – 165. https://doi.org/10.1016/S0921-5093(00)01292-2
7. **Greenwood, G.W., Johnson, R.H.** The Deformation of Metals under Small Stresses during Phase Transformations *Proceedings A* 283 (1394) 1965: pp. 403 – 422. https://doi.org/10.2307/2415276
8. **Leblond, J.B., Devaux, J.** Mathematical Modelling of Transformation Plasticity in Steels I: Case of Ideal-plastic Phases *International Journal of Plasticity* 5 (6) 1989: pp. 551 – 572. https://doi.org/10.1016/0749-6419(89)90001-6
9. **Leblond, J.B.** Mathematical Modelling of Transformation Plasticity in Steels II: Coupling with Strain Hardening Phenomena *International Journal of Plasticity* 5 (6) 1989: 573 – 591. https://doi.org/10.1016/0749-6419(89)90002-8
10. **Yanagisawa, Y., Kishi, Y., Sasaki, K.** Analysis of Residual Stresses during Heat Treatment of Large Forged Shafts Considering Transformation Plasticity and Creep Deformation *Strength of Materials* 49 (2) 2017: pp. 239 – 249. https://doi.org/10.1007/s11223-017-9863-7
11. **Yao, X., Zhu, L., Li, M.** A Fully Coupled Material Constitutive Model for Steel Quench Analysis *International Journal of Microstructure and Materials Properties* 5 (6) 2010: pp. 501 – 523. https://doi.org/10.1504/IJMMP.2010.038151
12. **Liu, C., Yao, K., Xu, X., Liu, Z.** Models for Transformation Plasticity in Loaded Steels Subjected to Bainitic and Martensitic Transformation *Materials Science and Technology* 17 (8) 2001: pp. 983 – 988. https://doi.org/10.1179/026708301101510825
13. **Lingamanaik, S.N., Chen, B.K.** The Effects of Carburising and Quenching Process on the Formation of Residual Stresses in Automotive Gears *Computational Materials Science* 62 2012: pp. 99 – 104. https://doi.org/10.1016/j.commatsci.2012.05.033
14. **Khan, D., Gautham, B.P.** Integrated Modeling of Carburizing-quenching-tempering of Steel Gears for An ICME Framework *Integrating Materials and Manufacturing Innovation* 7 2018: pp. 28 – 41. https://doi.org/10.1007/s40192-018-0107-x
15. Non-Destructive Testing-Test Method for Residual Stress Analysis by X-ray Diffraction, *European Standard EN15305*, 2008.
16. **Li, Y., Pan, J., Zhou, X., Li, Z.** Computer Simulation of Concentration Field of Over-carburizing *Material Science and Technology* 1 1999: pp. 22 – 26.
17. **Lee, S.J., Matlock, D.K., Tyne, C.J.V.** Carbon Diffusivity in Multi-component Austenite *Scripta Materialia* 64 2011: pp. 805 – 808. https://doi.org/10.1016/j.scriptamat.2011.01.001
18. **Saunders, N., Guo, U.K.Z., Li, X., Miodownik, A.P., Schillé, J.Ph.** Using JMatPro to Model Materials Properties and Behavior *JOM* 55 (12) 2003: pp. 60 – 65. https://doi.org/10.1007/s11837-003-0013-2
19. **Şimşir, C., Gür, C.H.** 3D FEM Simulation of Steel Quenching and Investigation of the Effect of Asymmetric Geometry on Residual Stress Distribution *Journal of Materials Processing Technology* 207 2008: pp. 211 – 221. https://doi.org/10.1016/j.jmatprotec.2007.12.074
20. **Sugianto, A., Narazaki, M., Kogawara, M., Shirayori, A., Kim, S.Y., Kubota, S.** Numerical Simulation and

Experimental Verification of Carburizing-quenching Process of SCr420H Steel Helical Gear *Journal of Materials Processing Technology* 209 2009: pp. 597 – 3609. https://doi.org/10.1016/j.jmatprotec.2008.08.017

21. **Narazaki, M., Okamura, T., Sichino, H.** Validation of Material Property Data by Comparison between Simulation and Experimental Results of Jominy End Quenching *Report B-1, JSHT & JSMS*, Kyoto, 2004.
22. **Taleb, L., Cavallo, N., Waeckel, F.** Experimental Analysis of Transformation Plasticity *International Journal of Plasticity* 17 (1) 2001: pp. 1 – 20. https://doi.org/10.1016/S0749-6419(99)00090-X
23. **Zhang, X., Tang, J., Zhang, X.** An Optimized Hardness Model for Carburizing-quenching of Low Carbon Alloy Steel *Journal of Central South University* 24 (1) 2017 pp. 9 – 6. https://doi.org/10.1007/s11771-017-3403-2
24. **Qin, S.W., Zhang, B., Zhao, H.H., Zhang, Y.F.** Effect of Phase Change Plasticity Coefficient on Residual Stress of 18CrNimo7-6 Carburized Carbon Steel *Surface Technology* 49 (12) 2020: pp. 138 – 143. https://doi.org/10.16490/j.cnki.issn.1001-3660.2020.12.015
25. **Woods, J.L., Daniewicz, S.R., Nellums, N.** Increasing the Bending Fatigue Strength of Carburized Spur Gear Teeth by Presetting *International Journal of Plasticity* 21 1999: pp. 549 – 556. https://doi.org/10.1016/S0142-1123(99)00011-0
26. **Selcuk, B., Leak, R., Karamic, M.B., Kuzucu. V.** An Investigation on Surface Properties of Treated Low Carbon and Alloyed Steels (Boriding and Carburizing) *Journal of Materials Processing Technology* 103 2000: pp. 310 – 317. https://doi.org/10.1016/S0924-0136(99)00488-4
27. **Denis, S.** Considering Stress-Phase Transformation Interactions in the Calculation of Heat Treatment Residual Stresses *Journal de Physique Iv* 6 (1) 1996: pp. 293 – 317. https://doi.org/10.1007/978-3-7091-2660-8_10
28. **Yang, Q., Ren, X., Gao, Y., Li, Y., Zhao, Y., Yao, M.** Effect of Carburization on Residual Stress Field of 20CrMnTi Specimen and Its Numerical Simulation *Materials Science and Engineering: A* 392 2005: pp. 240 – 247. https://doi.org/10.1016/j.msea.2004.09.027